C. R. Mecanique 340 (2012) 57–66

Contents lists available at SciVerse ScienceDirect

Comptes Rendus Mecanique

www.sciencedirect.com

Biomimetic flow control

Stall control with feathers: Self-activated flaps on finite wings at low Reynolds numbers

C.H. John Wang, Jörg Schlüter

School of Mechanical and Aerospace Engineering, College of Engineering, Nanyang Technological University, Singapore

ARTICLE INFO

Article history:
Available online 30 December 2011

Keywords:
Passive high lift device
MAV
Wind tunnel

ABSTRACT

We present experimental data on the use of a "pop-up feather" type high lift device (passive flap) on the upper side of the wing. While a number of previous studies have shown the effectiveness of this flap in two-dimensional geometries, we focus here on the use of the flap on finite wings and the three-dimensional flows involved in these geometries. We present parameter studies to determine the optimal size and location of such a flap on a rectangular SD8020 finite wing. We show that the flap has virtually no effect on the wing tip and that the optimal placement of the flap near the wing root is close to the optimum found in two-dimensional airfoil studies.

1. Introduction

Biological examples have long been an inspiration for mankind. The flight of birds and insects directed innovation towards the development of aircraft as it demonstrated that flying is indeed possible. Due to the long periods of evolution, nature has developed flow control mechanisms that are less obvious from an engineering perspective, but can be applied to wide variety of engineering designs. The inspiration from nature proved to be especially helpful when designing for passive flow control mechanisms, such as the shark skin suit that has been used by Olympic swimmers. Another interesting flow control device is that of the bird covert-feather on the upper side of the bird's wing as shown in Fig. 1. These feathers can be emulated by an artificial bird feather type movable flap described by Bechert et al. [1].

The "artificial bird feather" style movable flap, or passive flap device, promises to be particularly useful as a lift enhancement device for small and light-weight aircraft where space and weight are critical to the success of the aircraft. The implementation of a light and effective high lift device with minimal mechanism involved is especially important when it comes to designing Micro Air Vehicles (MAV), where the use of conventional aircraft design encounters a performance reduction due to the Reynolds number effect: as the Reynolds number decreases, the stall angle, and the maximum lift coefficient, decrease with it [2]. The use of the passive flap is therefore an attractive choice, as it does not require activation devices. The adaptation of the passive flap onto MAV is not exactly straight forward, however, as flow separation location, flow condition, wing configuration, and size of the passive flap all effect its performance.

2. Background

The inspiration for the passive flap device, as documented by Liebe in his 1979 article [3], came from the observation of landing birds: as the bird repositioned itself for landing, secondary covert-feathers from the upper-wing surface would levitate from their original position and form recirculation pockets as shown in Fig. 1. The repositioning of the wing increased its effective angle of attack, causing flow separation along the upper wing. The reversed flow within the turbulent

E-mail addresses: m080031@ntu.edu.sg (C.H.J. Wang), schluter@ntu.edu.sg (J. Schlüter).

1631-0721/$ – see front matter
doi:10.1016/j.crme.2011.11.001

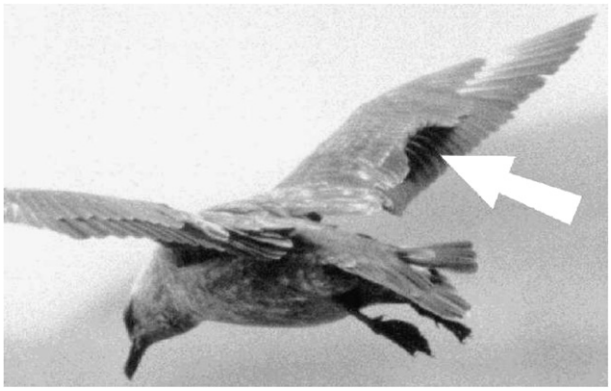

Fig. 1. Picture of a bird moments before it lands, showing displaced greater secondary covert-feathers [4].

Fig. 2. Illustration of the passive flap device and its effect on the free stream flow. The recirculation zone has been exaggerated to show the flow direction.

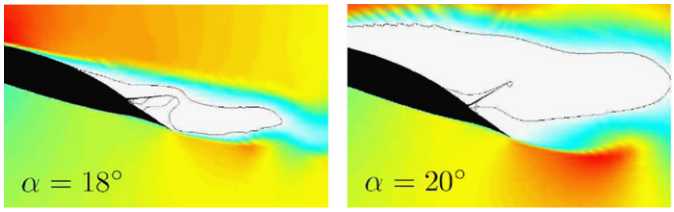

(a) $\beta = 40°$ (b) $\beta = 66°$

Fig. 3. Simulated x-velocity profile of passive flaps at fixed deflection angle (β) subjected to different angle of attacks (α) [4].

separation region creates enough pressure difference to push the covert-feather upward, creating smoother upper-wing profile, redirecting the airflow over the wing and reducing local flow separation as shown in Fig. 2.

Further research on the passive flap was conducted by Bechert et al. [1] in order to adapt the passive flap concept into workable device. After evaluating the wind tunnel data for the device's reliability and susceptibility to hysteresis in flap motion, a single flap in the aft-section of the airfoil was chosen for full-size flight test at $Re = 1.25 \times 10^6$. Although only 61% of the span was fitted with the passive flap in order to maintain controllability, the flight test still yields a 7% increase in maximum lift. Perhaps the most in-depth analysis of the fluid-induced motion experienced by the passive flap device is provided by the follow-up study from Schatz et al. [4]. Computational fluid dynamics (CFD) analysis was used to provide visualization for velocity and pressure field surrounding the passive flap and the HQ17 airfoil. Fig. 3 shows the mean x-velocity (free stream direction) flow field around passive flaps.

Although the device is not at the equilibrium deflection angle as part of the flow field analysis, the plots provided a clear picture of the pre-separation laminar attached flow, the turbulent separation region behind the flap and the airfoil, as well as the recirculation flow between the passive flap and the free stream flow. The partially deployed passive flap still produces additional mean lift generation, but to a lesser extent compared to the fully extended one. At low Reynolds numbers, the stall becomes even more complex, as the flow separation occurs in a laminar regime, sometimes accompanied by a recirculation bubble. As the stall occurs at lower angles-of-attack, low Reynolds number airfoils benefit particularly from the passive flap, as shown by Kernstine et al. [5] and Schlüter [6], with the later confirming the performance gain from to the passive flap under low Reynolds number condition ($Re = 3 \times 10^5$ and $Re = 4 \times 10^4$, respectively), and reported as much as 50% increase in maximum sectional lift coefficient on SD8020 airfoil. The dye visualization (Fig. 4) performed in water tunnel by Schlüter also confirmed that the laminar separation bubble develops into fully turbulent separation region post-stall. Further 2D experiments with pressure tap readings were conducted by Johnston et al. [7].

All studies on this subject have so far addressed only the effect of the flaps on two-dimensional airfoil geometries. The only exception is the flight test of Bechert et al. [1], which was limited to a proof-of-concept kind of study. Since the stall on a finite wing does not occur uniformly along the wingspan, the application of the flap on a finite wing aircraft is not straight-forward. The wing-tip vortices reenergize the flow at the tips and delay stall significantly. Hence, the flow is inherently highly three-dimensional as the stall regime at the wing root is more advanced than towards the wing tips.

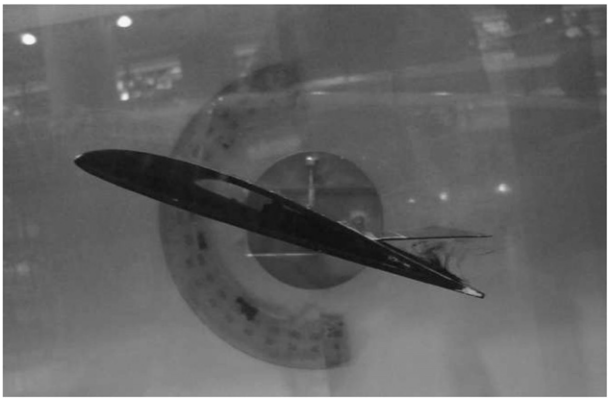

Fig. 4. Dye based visualization for SD8020 with $\alpha > \alpha_{stall}$, showing the attached flow at the upper surface and the turbulent separation behind the flap [6].

The stall becomes even more complex, if geometric or aerodynamic twist is involved. To approach the issue of three-dimensionality on the deployment of a passive flap on a finite wing geometry, we present here parameter studies on a generic finite wing model to determine the factors of size and location of the flap on the lift characteristics. Section 3 describes the experimental setup and procedures as well as the models used. Section 4 presents and discusses the results, while we summarize our findings in Section 5.

3. Experimental setup

Experiments were conducted in the Nanyang Technological University Wind Tunnel lab using the 1.1 m × 0.9 m low speed wind tunnel, and the aerodynamics data was taken using a 6-component internal force balance.[1] The NTU Low Speed Wind Tunnel has a contraction ratio of 6.17. The flow turbulence intensity has been measured to be below 1% and the flow uniformity inside the test section was determined to be 98.5% at 10 m/s. The 6-component internal force balance has a data acquisition range of up to 50 N for side and lift forces, 20 N for drag force, and 5 N-m for moment measurement; the accuracy of the instrument is 0.1% of the full range for each of the components. Fig. 5 presents the photos of the equipment used.

We used two different wind tunnel models. The first model is a straight-wing balsa model using SD8020 profile with a chord-length of 0.1 m and a span of 0.5 m; the second is a foam-based commercial glider-racer model as shown in Fig. 5(c). The passive flap device was modeled with uni-directional (span-wise) carbon fiber strips hinged to the wing model using clear plastic tape. The choice of flap material was based on previous experimental studies conducted here in NTU [6], and is considered as fully rigid for the purpose of this study. The majority of the experiments are conducted at $Re = 4 \times 10^4$, which corresponds to 6.4 m/s. The model and the flap configurations used in the experiment are shown in Fig. 6.

To demonstrate the accuracy of the balance, we compare our measurements of the finite wing SD8020 with the airfoil data of Selig et al. [8]. Here, we have corrected the literature data for finite wing effects using Eq. (1) with an efficiency factor of $e = 0.9$. The comparison of the model lift curve with literature data is shown in Fig. 7.

$$C_{L,\alpha} = \frac{C_{l,\alpha}}{57.3 \times \frac{C_{l,\alpha}}{\pi e AR}} \tag{1}$$

4. Results and discussion

4.1. The effect of flap span

As the effective angle of attack is different along the span of the wing, the summation of forces acting on the flap, and hence the flap angle, is not representative of the flow separation throughout the wing. Since the difference in lift distribution along the wingspan is largely due to the wing-tip vortex flow, it would be interesting to see how shrinking of the flap towards the center body effects the performance of the device. Sets of 30 mm carbon fiber strips were used for flap in this experiment, and are installed with the front of the flap located at 70%, 60%, and 50% x/c ($0.7C$, $0.6C$, and $0.5C$). A total of 4 flap setups were used, with the flap spanning 40%, 60%, 80%, and 100% of the wing. The experimental results are compiled below with Fig. 8 showing the best single flap results while Fig. 9 and Fig. 10 contain the rest of the data.

The experimental results indicated that by shortening the span of the flap, it is possible to reduce the amount of down-wash force acting on the flap, so that while the flapped wing area is reduced, overall lift generation increased. Reducing the

[1] Drag data was not used as low angle of attack data falls below the instrument accuracy.

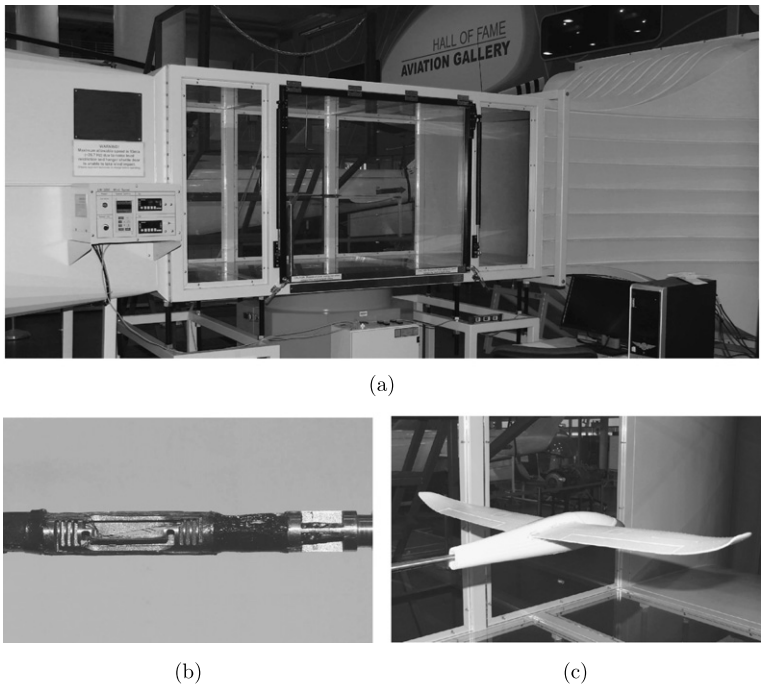

Fig. 5. Pictures of the wind tunnel (a), internal force balance (b), and the practical study aircraft model (c).

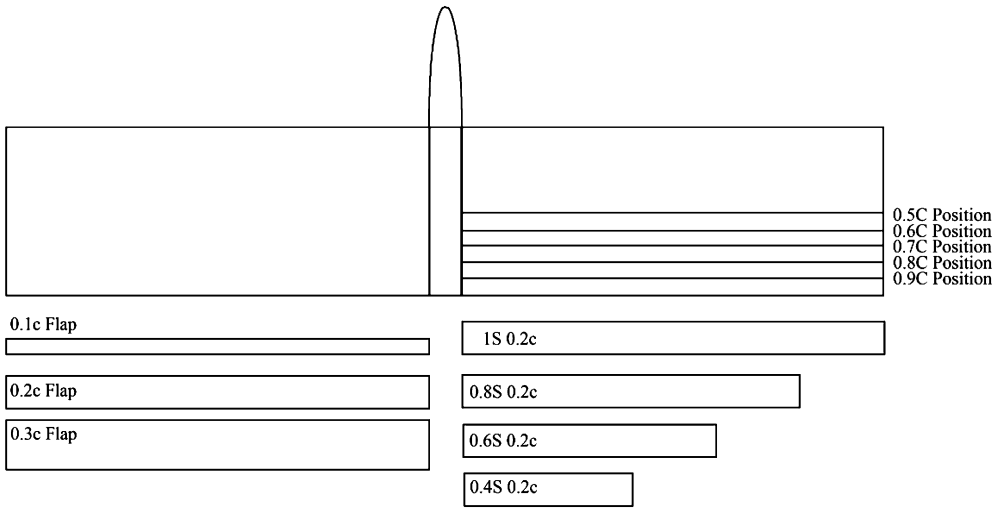

Fig. 6. Schematic of the straight-wing aircraft model showing the designation used for flap positioning (C), flap chord-length (c), and flap-span configuration (S).

flap span too much, on the other hand, resulted in reduced contribution to lift generation; the reduction of lift is expected as the flap size decreases, though the increased contribution from the flow field around the aircraft body on flap could have worsen the performance dip. For the single flap experiment, the optimal setup was observed to be the 0.8S flap.

In addition to the single flap configurations covered in 0.1c and 0.3c experiments, the 0.2c experiment contains an extra set of composite-flap setup. The additional flap configuration consists of a 0.6S flap on the inner portion of the wing supplemented by a 0.4S flap on the outer portion. The idea behind this setup is that the outer flap would delay stall so a higher combined lift generation could be achieved.

The composite-flap configuration performed significantly better than a single 0.6S flap, which by itself barely produces any lift increase; it also outperformed all other single flap configurations. It appears that the outer flap has a positive effect on the lift distribution over the wing and lessens the effect of down-wash on the inner flap, resulting in an overall increase in lift generation. As the composite-flap configuration was added in at the last minute as a proof-of-concept test, the data available for analysis is limited to the sets displayed above.

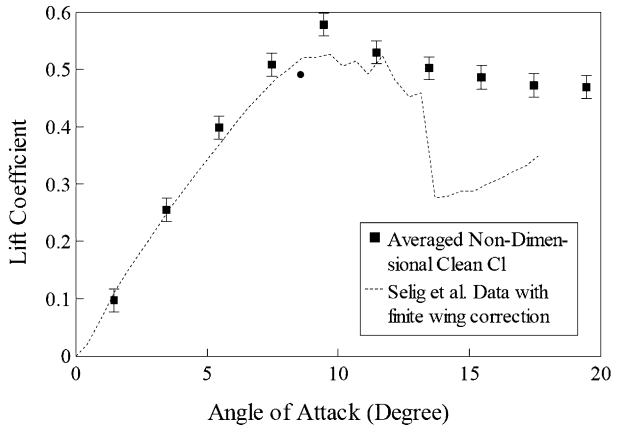

Fig. 7. Comparison of wing model lift curve with data from Selig et al. [8].

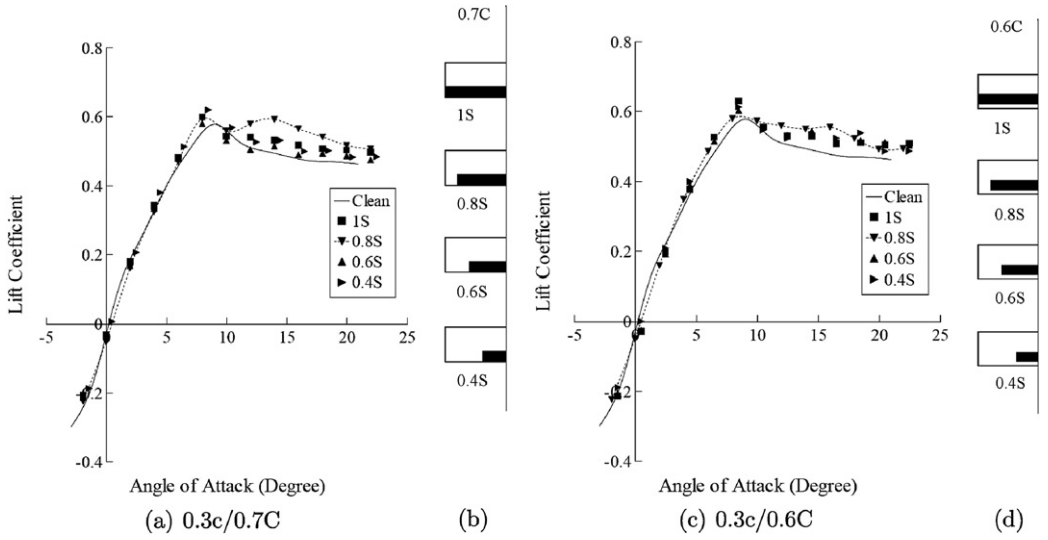

Fig. 8. Lift curves of 0.3c passive flaps with different span-wise sizing (illustrated in (b) and (d)) at $Re = 4 \times 10^4$. The leading edges of the flaps are located at 70% x/c and 60% x/c for (a) and (c) respectively.

4.2. The effect of flap position

Since the deployment of the passive flap is triggered by flow separation, the optimal positioning of the flap would depend on the separation point of the airfoil and, in the case of larger flap sizes, the size of the separation zone. Like most thin airfoil the SD8020 exhibits leading edge stall, meaning that a well placed passive flap will be able to create enough pull to redirect the free stream flow that prevents the abrupt drop in lift. The flap position experiments were conducted from the tailing-edge flushed position[2] to mid-chord with a 0.1c increment, with a constant flap chord of 0.3c. The results are shown in Fig. 11.

The data collected showed a slightly better flap performance as the flap position shifted forward until 0.6C, with the flap located at 0.5C failing to lift up even at very high angle of attack. It appears that, at least for the SD8020 finite wing model, the chord-wise position has very little influence on the performance of the passive flap as long as the flow field is favorable to the deployment of the flap. It should be noted that no experiments were done for flap position past mid-chord as the flap was unable to conform to the curvature of the airfoil and would drastically alter its aerodynamic characteristics.

4.3. The effect of flap chord-length

As the passive flap is lifted by the recirculation flow, its movement is constrained to within the separation zone. The confinement to the separation zone means that larger flap size could completely cut the flow separation in two, and it

[2] Where the trailing edge of the flap is flushed with the trailing edge of the wing.

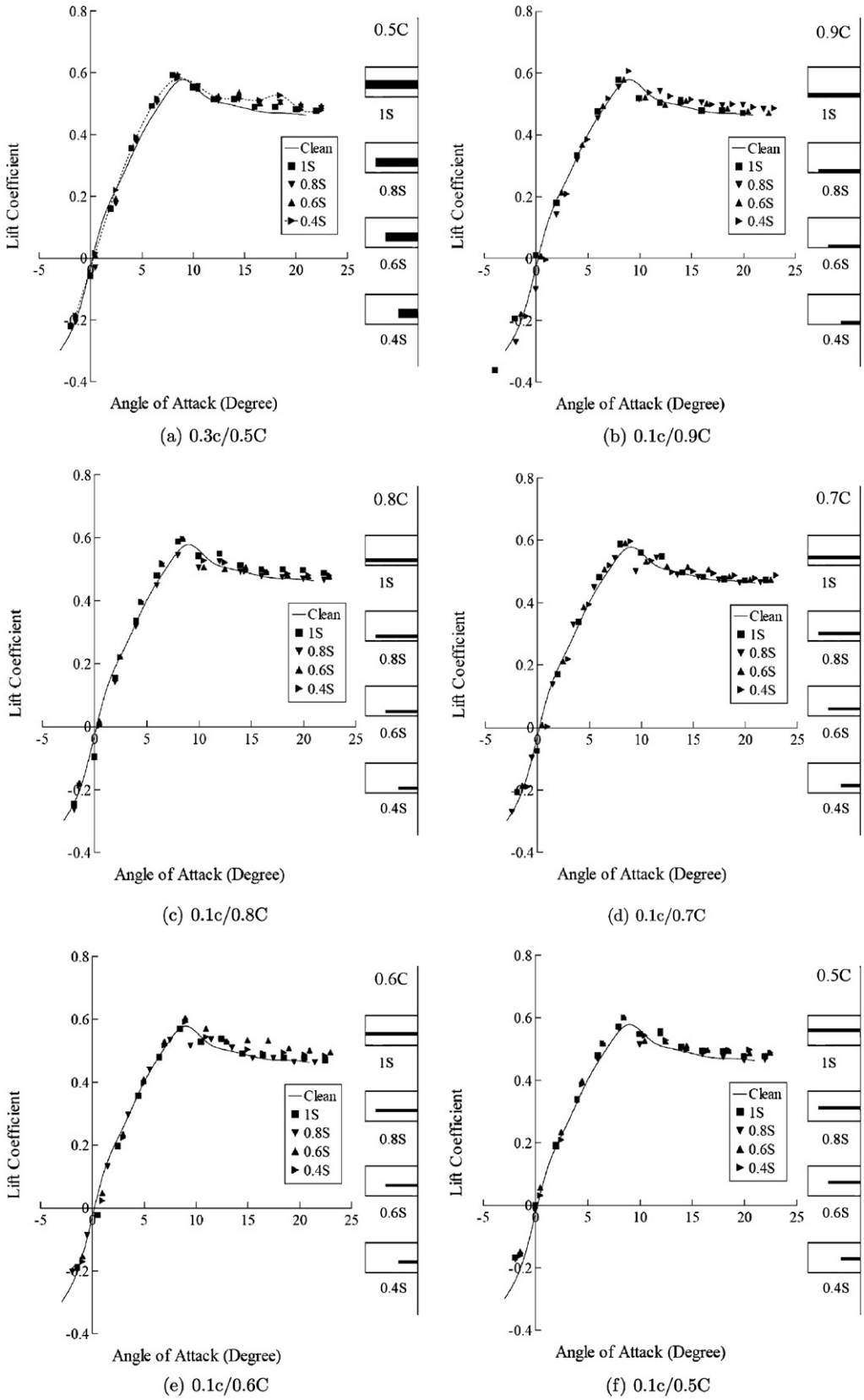

Fig. 9. Lift curves of passive flaps with different flap spans at $Re = 4 \times 10^4$.

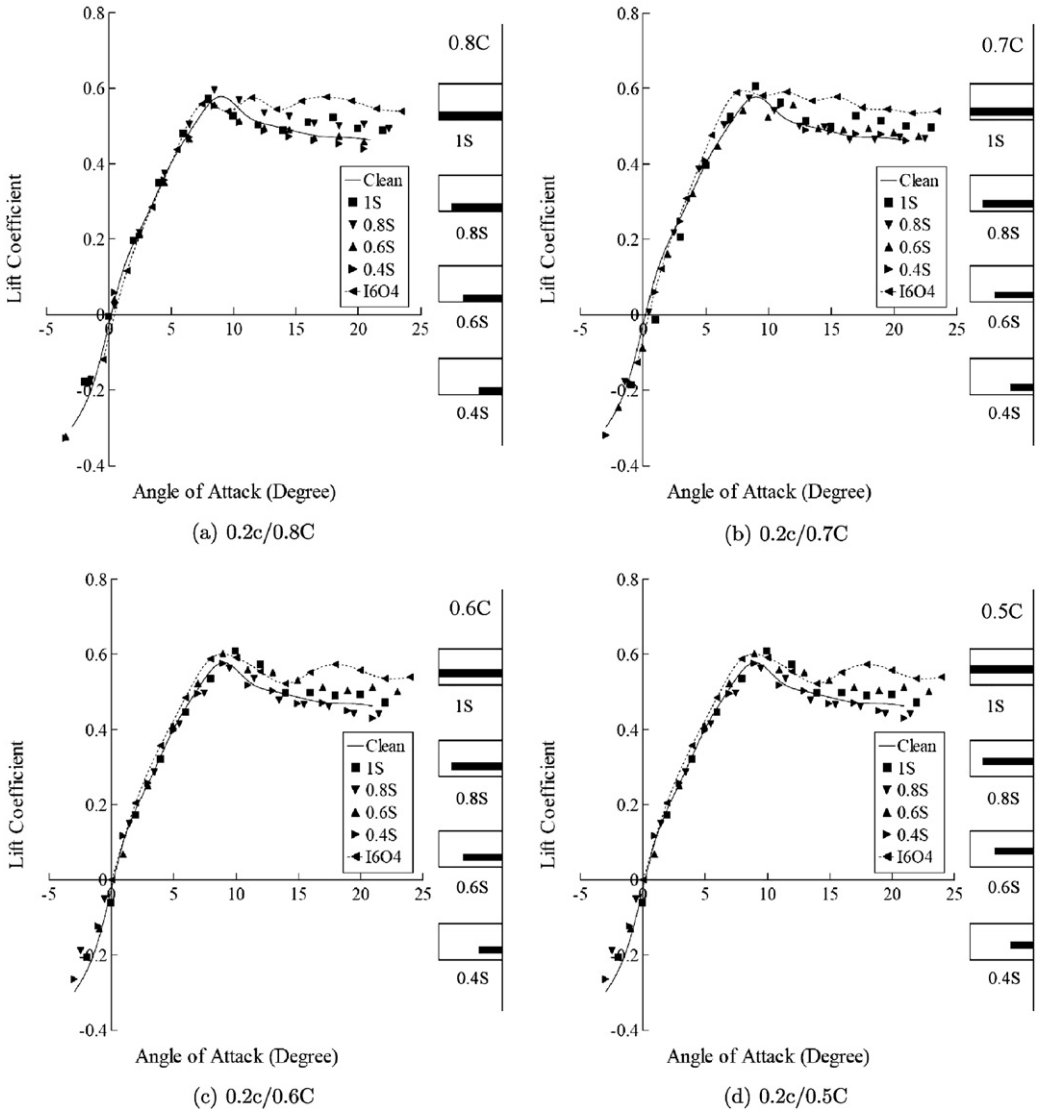

Fig. 10. Lift curves of 0.2c passive flaps at $Re = 4 \times 10^4$.

would be interesting to compare the performance to that of a smaller flap with its partially separated flow field. It would be interesting to find out if the recirculation flow diversion from a smaller flap is capable of achieving the same lift increase as a larger flap. Fig. 12 shows the results.

Judging from Fig. 12(b), the flap's chord size plays an important role in the passive flap performance when subjected to three-dimensional flow. The 30 mm flaps achieved $\sim$ 18% lift recovery at 15 degree angle of attack, while the 20 mm flaps managed around half of that. The 10 mm flap does not appear to have significant effect on the lift. The difference in lift recovery might be due to the difference in the size of the resulting recirculation flow: larger flap diverts more airflow behind it, causing a stronger recirculation flow that is more capable of pulling the free stream flow down and create more lift. It should be noted that the complete reversal (tipping-over) of the flap was observed at very high angle of attack, and would result in hysteresis in lift curve as the flipped flap is unable to contribute to the lift generation; the reversal of the flaps cannot be self-corrected until flow reattachment occurred. To counter the phenomenon, a passive flap angle limiter should be used.

4.4. The effect of Reynolds number

The actual operation of the MAV would not be confined to a single Reynolds number, so a good lift enhancement device should maintain its performance throughout the operational Reynolds number range. Higher Reynolds number, and hence higher free stream velocity, could produce a more powerful recirculation flow that results in a larger flap displacement.

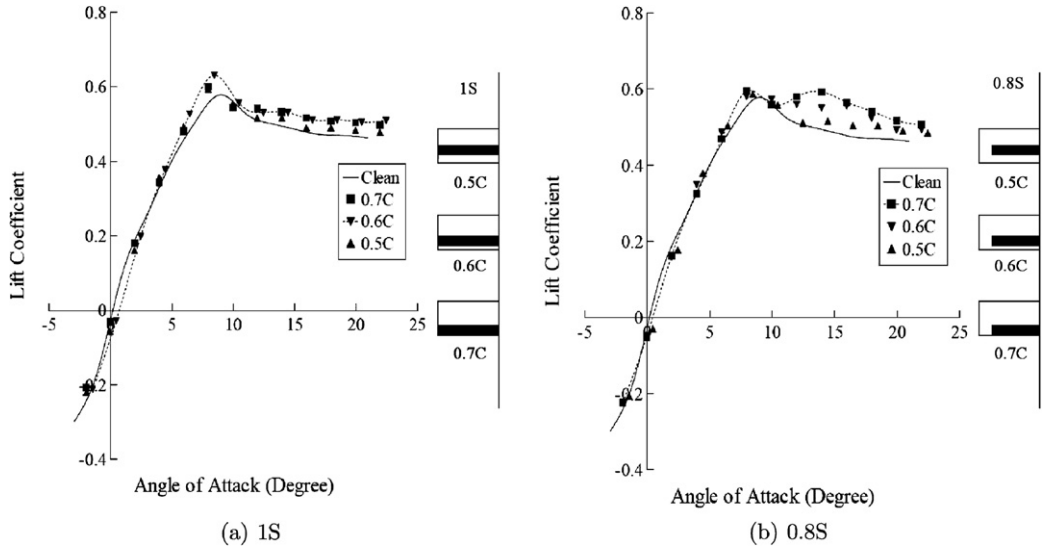

Fig. 11. Lift curves of 0.3*c* passive flaps at different chord-wise position at $Re = 4 \times 10^4$.

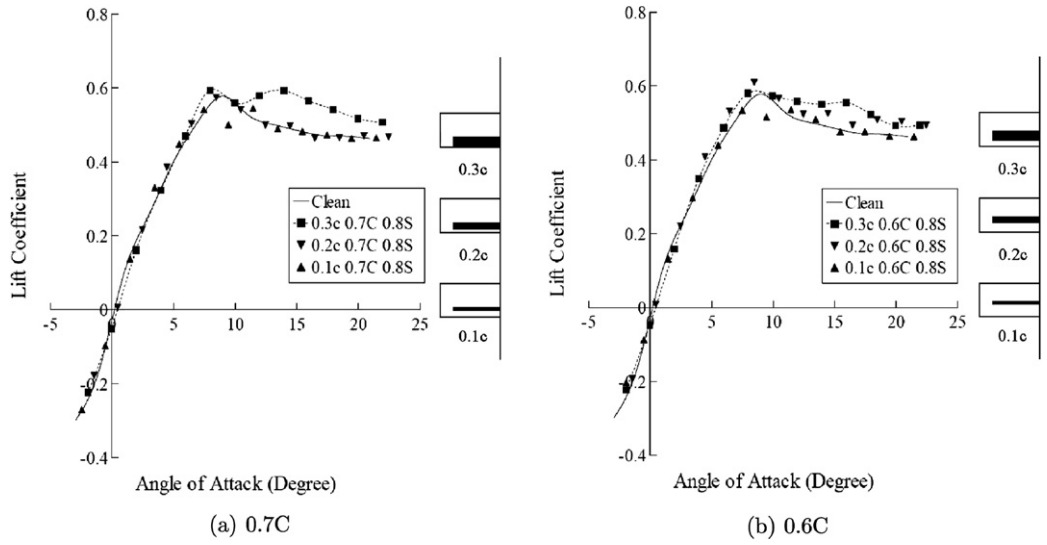

Fig. 12. Lift curves of 0.8*S* passive flaps with various flap chord-length at $Re = 4 \times 10^4$ compared with data without the flap. The flaps are positioned at 0.7*C* for (a) and 0.6*C* for (b).

Kernstine et al. [5] reported a positive effect of Reynolds number on lift enhancement from their tests at $Re = 1.66 \times 10^5$ and $Re = 4.53 \times 10^5$, further testing on the subject was limited by their flap material. For this experiment, a flap with a chord-length of 20% chord and 30% chord which span 80% of the wing (0.8*S*) were used[3]; experiments were conducted at $Re = 4 \times 10^4$, $Re = 5 \times 10^4$, and $Re = 6 \times 10^4$. The results are reported in Fig. 13.

The plot demonstrated the effect of Reynolds number on the maximum lift coefficient of the clean airfoil, which caused a slightly delayed post-stall recovery at higher Reynolds number for flaps with the same chord-wise location and flap chord-length. The Reynolds number experiment showed mixed results, while higher Reynolds number generates a higher lift coefficient post-stall, the relative increase in lift is less. We associate the lower lift increase for the $Re = 60{,}000$ case to the delay in flow separation, and hence the delay in passive flap deployment; the pressure distribution of the low Reynolds number airfoil could also have an effect on the passive flap performance at higher Reynolds number.

[3] Flap configuration denoted in (flap chord)/(flap position) form.

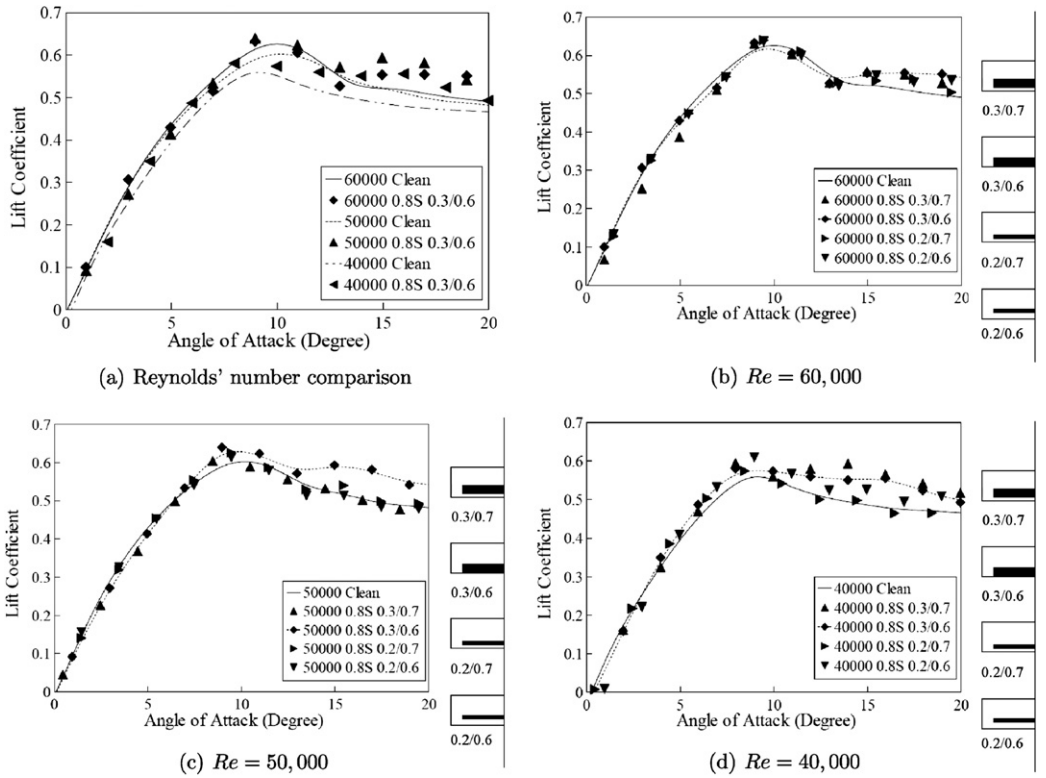

Fig. 13. Lift curves of wings with passive flap at various Reynolds number compared to that of clean wings at the same Reynolds number.

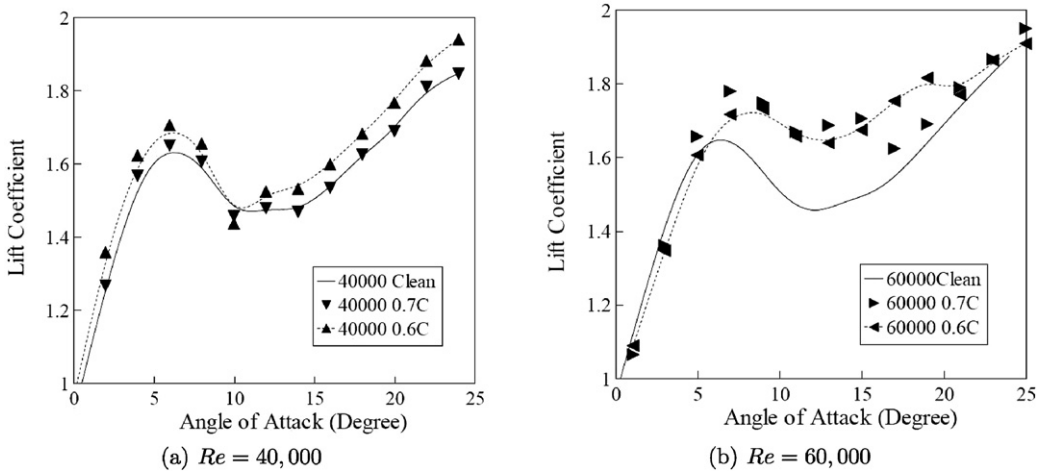

Fig. 14. The lift curve of the aircraft mode with and without the passive flap device installed at $Re = 40{,}000$ and $Re = 60{,}000$.

4.5. Full model results

Additional experiments were performed inside the wind tunnel on a Multiplex Merlin electric racer model over selected operational Reynolds number range of the aircraft. The aim of the study was to provide insight on the performance gain achievable when retrofitting existing aircraft design with the passive flap device. As the airplane model has a wing profile of a thin airfoil with small camber, the type of stall encountered should be similar to that of the SD8020 wing model, so the model was fitted with a 0.3*c* flap at 0.7*C* and 0.6*C* position. The flap span was chosen to cover the portion of the wing with structural spar under the foam wing to prevent the effect of wing deformation on flap deployment. The experimental results are shown in Fig. 14.

It appears that the recirculation flow at $Re = 40{,}000$ is insufficient to overcome the weight of the flap, and no flap deployment was observed at this Reynolds number. On the other hand, the flap performance at $Re = 60{,}000$ lived up to

the expectation and produced significant lift increase. It should be noted that flap-tipping was observed at 20 degree angle of attack as the airflow detached from the passive flap. The phenomenon is unlikely to be observed in actual flight as it occurred way past the regular stall angle, although flap angle limiter could be installed to address safety concern.

5. Conclusions

We have conducted a series of experiments to approach the three-dimensional effects on the performance of a passive flap on a finite wing. The parameter studies that we performed show that the flap close to the wing tip has no or only minor effects. We conclude that the best performance from the flap can be gained when it covers around 80% of the wingspan, leaving the 20% next to the wing tip clear. The placement of the size and chord-wise location of the flap seems to follow results obtained by two-dimensional airfoil analysis, albeit the fact that the overall performance gain for three-dimensional geometries is lower than observed for two-dimensional airfoil analysis. The best performing single flap configuration for the model appears to be the $0.3c/0.7C/0.8S$ setup.

The current study provides valuable validation data for future computational studies that are able to derive a more detailed picture on the flow pattern of three-dimensional geometries with passive flaps. We have also shown that this biologically inspired high lift device has a real potential to be applied to realistic MAV designs, as high lift coefficient and gentle stall characteristic are achieved with negligible investment in cost and weight of the aircraft.

References

[1] D.W. Bechert, M. Bruse, R. Meyer, W. Hage, Biological surfaces and their technological application – laboratory and flight experiments on drag reduction and separation control, AIAA 97-1960, 1997.
[2] T.J. Müller, J.D. DeLaurier, An overview of micro air vehicle aerodynamics, in: T.J. Müller (Ed.), Fixed and Flapping Wing Aerodynamics for Micro Air Vehicle Applications, in: Progress in Astronautics and Aeronautics, vol. 195, AIAA, 2001, pp. 1–10.
[3] W. Liebe, Der Auftrieb am Tragflügel: Entstehung und Zusammenbrunch, Aerokurier 12 (1979) 1520–1523.
[4] M. Schatz, T. Knacke, F. Thiele, R. Meyer, W. Hage, D. Bechert, Separation control by self-activated movable flaps, in: 42nd AIAA Aerospace Sciences Meeting & Exhibit, Reno, NV, 2004.
[5] K.H. Kernstine, C.J. Moore, A. Cutler, R. Mittal, Initial characterization of self-activated movable flaps, "Pop-Up Feathers", in: 46th AIAA Aerospace Sciences Meeting & Exhibit, Reno, NV, 2008.
[6] J. Schlüter, Lift enhancement at low Reynolds numbers using pop-up feathers, in: 39th AIAA Fluid Dynamics Conference, San Antonio, TX, 2009.
[7] J. Johnston, A. Gopalarathnam, J. Edward, Experimental investigation of bio-inspired high lift effectors on a 2-D airfoil, in: 29th AIAA Applied Aerodynamics Conference, Honolulu, Hawaii, 2011.
[8] M. Selig, J. Guglielmo, A. Broern, P. Giguere, Experiments on airfoils at low Reynolds' numbers, AIAA 96-0062, 1996.